IPOL IMAGE PROCESSING ON LINE

Published in Image Processing On Line on 2024–06–23.
Submitted on 2024–02–21, accepted on 2024–05–24.
ISSN 2105–1232 © 2024 IPOL & the authors CC–BY–NC–SA
This article is available online with supplementary materials,
software, datasets and online demo at
https://doi.org/10.5201/ipol.2024.530

Dehazing with Dark Channel Prior: Analysis and Implementation

Jose-Luis Lisani[1], Charles Hessel[2]

[1]Universitat Illes Balears, Spain (joseluis.lisani@uib.es)
[2]Université Paris-Saclay, ENS Paris-Saclay, Centre Borelli, Gif-sur-Yvette, France
(charles.hessel@ens-paris-saclay.fr)

Communicated by Gregory Randall *Demo edited by* Jose-Luis Lisani

Abstract

In outdoor scenes, atmospheric absorption and scattering attenuate the radiance received by the camera and may produce haze. In 2009 He et al. proposed a simple but effective dehazing algorithm based on a hypothesis called the 'dark channel prior' (DCP). Based on this prior several other dehazing methods have been published in recent years. In this paper we review the original algorithm by He et al., together with some posterior improvements proposed by the same and other authors. We also analyze the effect of the parameters on the results and we study a variant of the method proposed by Drews et al. for the analysis of haze in underwater images.

Source Code

The reviewed and documented source code and an online demo are available at the web page of this article[1]. Compilation and usage instructions are included in the README.txt file of the archive.

Keywords: haze removal; dark channel prior; underwater images

1 Introduction

Haze, fog or smoke (*haze* in general) are phenomena that may occur in outdoor scenes and that produce a reduction of the overall contrast of the image and a loss of color fidelity. This degradation is due to the absorption and scattering that the light suffers from when it travels through the atmosphere before reaching the camera.

Since the amount of haze at a given pixel of the image depends on the distance from the scene to the camera (the *depth*), which is generally unknown, haze removal is a challenging problem.

[1]https://doi.org/10.5201/ipol.2024.530

Although some solutions have been proposed for single image dehazing based on different assumptions [4, 13], the majority of current methods are based on the *dark channel prior* (DCP) hypothesis, first proposed by He et al. in [5, 6].

In this paper we shall review He et al.'s method for haze removal. In Section 2 we will describe the image formation model on which the model is based. The dark channel prior shall be presented in Section 3, together with the dehazing algorithm proposed by the authors. Several experiments with different values of the algorithm's parameters are shown in Section 4. Some variations of the method will be discussed in Section 5. Finally, some conclusions are drawn in Section 6.

2 Image Formation Model

The most common model describing the formation of an image in a scene captured in a isotropic homogeneous medium (atmosphere, water, etc.) is [8, 10, 11]

$$\boldsymbol{I}(\boldsymbol{x}) = \boldsymbol{I}_d(\boldsymbol{x}) + \boldsymbol{I}_{fs}(\boldsymbol{x}) + \boldsymbol{I}_{bs}(\boldsymbol{x}), \tag{1}$$

where $\boldsymbol{I} = (I^R, I^G, I^B)$ is the observed intensity, obtained as the addition of three components: the direct illumination $\boldsymbol{I}_d$, the forward-scattering $\boldsymbol{I}_{fs}$ and the backscattering $\boldsymbol{I}_{bs}$.

The direct illumination is the fraction of the light reflected in the scene objects that reaches the camera. It is defined as

$$\boldsymbol{I}_d(\boldsymbol{x}) = \boldsymbol{J}(\boldsymbol{x}) e^{-\eta d(\boldsymbol{x})}, \tag{2}$$

where $\boldsymbol{J} = (J^R, J^G, J^B)$ is the scene radiance, d is the depth, and η is the attenuation coefficient of the medium. In outdoor scenes $\eta = \beta$, the scattering coefficient of the atmosphere; in underwater environments η is the sum of the absorption and scattering coefficients of the water [8]. In general, the value of η depends on the wavelength of the light, however, for fog and dense haze it can be approximated by a constant [11]. The term $e^{-\eta d(\boldsymbol{x})}$ is usually denoted as $t(\boldsymbol{x})$ and is called the *medium transmission map*. Note that the value of the transmission depends on the depth: higher values indicate that the objects are closer to the camera, while lower values are associated to further regions in the scene.

The forward-scattering term refers to the light reflected by the scene objects which has been scattered, with a small angle, in the direction of the observer [8]. Its value is small compared to the backscattering term and is usually neglected.

The backscattering $\boldsymbol{I}_{bs}$ (or *airlight* following the notation of [5, 6]), is caused by the scattering of the ambient illumination by particles in the medium and leads to shifts in the scene color. It can be expressed as

$$\boldsymbol{I}_{bs}(\boldsymbol{x}) = \boldsymbol{A}(1 - e^{-\eta d(\boldsymbol{x})}) = \boldsymbol{A}(1 - t(\boldsymbol{x})), \tag{3}$$

where $\boldsymbol{A} = (A^R, A^G, A^B)$ is the global light in the scene.

In summary, the interaction between the ambient light, the medium and the scene can be written as

$$\boldsymbol{I}(\boldsymbol{x}) = \boldsymbol{J}(\boldsymbol{x}) t(\boldsymbol{x}) + \boldsymbol{A}(1 - t(\boldsymbol{x})). \tag{4}$$

If the transmission $t(\boldsymbol{x})$ and the global illumination A are known, the scene radiance $\boldsymbol{J}$ can then recovered as

$$\boldsymbol{J}(\boldsymbol{x}) = \frac{\boldsymbol{I}(\boldsymbol{x}) - \boldsymbol{A}}{t(\boldsymbol{x})} + \boldsymbol{A}. \tag{5}$$

In [5, 6] He et al. propose a method for the estimation of $t(\boldsymbol{x})$ and $\boldsymbol{A}$ and then apply Equation (5) to recover the radiance. We shall review this method in the next section.

3 Haze Removal Using the Dark Channel Prior

Following Equation (4) we have that, if for a given pixel $\boldsymbol{x}$ of the scene $t(\boldsymbol{x}) = 0$, then $\boldsymbol{A} = \boldsymbol{I}(\boldsymbol{x})$. As a consequence, if the transmission map is known, A can be easily estimated (provided that $t(\boldsymbol{x}) = 0$ for some pixel. In practice, the process is slightly more complex, see Algorithm 1 for details). Therefore, the main difficulty in haze removal problems is the estimation of $t(\boldsymbol{x})$.

He et al. propose a simple method for this estimation, based on the following empirical observation: in a haze-free image not containing the sky, the minimum value of the image is zero at least for one of its channels (in grayscale images, the same observation is valid for the intensity channel). To corroborate this hypothesis they define an auxiliary one-channel image, called the *dark channel*

$$J^{\text{dark}}(\boldsymbol{x}) = \min_{\boldsymbol{y}\in\Omega(\boldsymbol{x})} \min_{c\in\{R,G,B\}} J^c(\boldsymbol{y}), \tag{6}$$

where J^c is the radiance of color channel c and $\Omega(\boldsymbol{x})$ is a square patch centered at $\boldsymbol{x}$. Note that if the scene is free of haze $J^c = I^c$ for the non-sky pixels.

According to the above hypothesis this dark channel image should be 0 for all the pixels not belonging to the sky (the *dark channel prior*). The authors empirically checked this by computing the dark channel values for 5000 randomly selected haze-free images, using a patch size of 15× 15 pixels. In order to satisfy the conditions of the prior, the sky regions were previously cropped from these images. Moreover, the radiances were approximated by the actual intensities of the images. They analyzed the obtained dark channel intensities and concluded that about 75% of the pixels had zero values and that for 90% of them the value was below 25 (the intensities of the original images were in the range [0, 255]). This results agree with the hypothesized prior.

3.1 Estimation of the Ambient Light

The ambient light is dominant in the pixels of the image more affected by the haze. As a consequence of the hypothesis exposed in the previous section, in these pixels the dark channel prior does not hold, and they are characterized by having a large value in the dark channel image. He et al. take advantage of this fact and suggest a very simple method for the estimation of $\boldsymbol{A}$: they pick the 0.1% brightest pixels in the dark channel image and, from them, they select the one ($\boldsymbol{x}^*$) having the highest intensity in the input image $\boldsymbol{I}$. Finally $\boldsymbol{A} = \boldsymbol{I}(\boldsymbol{x}^*)$.

A slight variation of this strategy is proposed in https://github.com/He-Zhang/image_dehaze: $\boldsymbol{A}$ is computed as the average of the intensities of the top 0.1% brightest pixels in the dark channel. We use this second version (Algorithm 1) in our implementation. An optional modification is also implemented in the code: the exclusion of saturated pixels in the estimation of the ambient light (see Section 5 for more details).

3.2 Estimation of the Transmission

Let us consider Equation (4). If we apply the *min* operator over each square patch Ω centered at pixel $\boldsymbol{x}$, we get

$$\min_{\boldsymbol{y}\in\Omega(\boldsymbol{x})} I^c(\boldsymbol{y}) = \min_{\boldsymbol{y}\in\Omega(\boldsymbol{x})} \left(J^c(\boldsymbol{y})t(\boldsymbol{y}) + A^c(1 - t(\boldsymbol{y}))\right), \tag{7}$$

If we assume that *the transmission map is locally constant in each patch*, then we have that $t(\boldsymbol{y}) = t(\boldsymbol{x})$ for $\boldsymbol{y} \in \Omega(\boldsymbol{x})$. Therefore

$$\min_{\boldsymbol{y}\in\Omega(\boldsymbol{x})} I^c(\boldsymbol{y}) = t(\boldsymbol{x}) \min_{\boldsymbol{y}\in\Omega(\boldsymbol{x})} J^c(\boldsymbol{y}) + A^c(1 - t(\boldsymbol{x})). \tag{8}$$

Algorithm 1: Ambient Light Estimation

Input : input image $\boldsymbol{I}$ with N pixels
Input : dark channel J^{dark}
Parameters: percentage of pixels used for the estimation (p). Default: $p = 0.1\%$.
Output : ambient light $\boldsymbol{A}$

1 $J^{\text{dark}} \leftarrow Sort(J^{\text{dark}})$ //Sort increasing
2 $M = \lfloor \frac{p}{100} \cdot N \rfloor)$ //Number of pixels used for the estimation
//Compute average of input values
3 $\boldsymbol{A} \leftarrow \boldsymbol{0}$
4 $i = N - 1$ //Position of the brightest pixel in the sorted dark channel
5 $j = 0$ //Counter for the number of pixels selected for the estimation
6 **while** $i \geq 0$ ***and*** $j < M$ **do**
//OPTIONAL (see Section 5): apply lines 7, 8 and 9 only if $\boldsymbol{I}(i)$ is not saturated (exclusion of saturated pixels)
7 $\boldsymbol{A} \longleftarrow \boldsymbol{A} + \boldsymbol{I}(i)$ //Add pixel color
8 $j = j + 1$ //Increase counter
9 $i = i - 1$ //Decrease counter
10 $\boldsymbol{A} \longleftarrow \boldsymbol{A}/M$

By dividing each side of the equation by A^c we can write

$$\min_{\boldsymbol{y} \in \Omega(\boldsymbol{x})} \frac{I^c(\boldsymbol{y})}{A^c} = t(\boldsymbol{x}) \min_{\boldsymbol{y} \in \Omega(\boldsymbol{x})} \frac{J^c(\boldsymbol{y})}{A^c} + 1 - t(\boldsymbol{x}). \tag{9}$$

If we take the minimum of the above equation over all the channels we obtain

$$\min_{c \in \{R,G,B\}} \min_{\boldsymbol{y} \in \Omega(\boldsymbol{x})} \frac{I^c(\boldsymbol{y})}{A^c} = t(\boldsymbol{x}) \min_{c \in \{R,G,B\}} \min_{\boldsymbol{y} \in \Omega(\boldsymbol{x})} \frac{J^c(\boldsymbol{y})}{A^c} + 1 - t(\boldsymbol{x}). \tag{10}$$

By assuming that

$$t(\boldsymbol{x}) \min_{c \in \{R,G,B\}} \min_{\boldsymbol{y} \in \Omega(\boldsymbol{x})} \frac{J^c(\boldsymbol{y})}{A^c} \approx 0, \tag{11}$$

t can be estimated as

$$t(\boldsymbol{x}) \approx 1 - \min_{c \in \{R,G,B\}} \min_{\boldsymbol{y} \in \Omega(\boldsymbol{x})} \frac{I^c(\boldsymbol{y})}{A^c}. \tag{12}$$

He and al. justify Equation (11) as follows:

- if $\boldsymbol{x}$ belongs to a haze-free patch not located in the sky region of the image, or if the amount of haze is moderate, we consider that the dark channel prior (approximately) holds. This implies that $\min_{c \in \{R,G,B\}} \min_{\boldsymbol{y} \in \Omega(\boldsymbol{x})} J^c(\boldsymbol{y})$ is small, which combined with the fact that A^c is a positive value and $A^c > J^c$ leads to

$$\min_{c \in \{R,G,B\}} \min_{\boldsymbol{y} \in \Omega(\boldsymbol{x})} \frac{J^c(\boldsymbol{y})}{A^c} \approx 0, \tag{13}$$

  and (11) follows.

- if $\boldsymbol{x}$ belongs to a haze-free patch located in the sky region of the image, since the color of the sky is usually very similar to the ambient light then $I^c = A^c$ for all c. If $\boldsymbol{x}$ belongs to a patch

with a large amount of haze its color will also be very similar to the ambient light. In both cases

$$\min_{c\in\{R,G,B\}} \min_{\boldsymbol{y}\in\Omega(\boldsymbol{x})} \frac{I^c(\boldsymbol{y})}{A^c} \approx 1,$$

therefore (Equation (12)) $t(\boldsymbol{x}) \approx 0$ and (11) holds.

Improving the estimate. A small modification of Equation (12) is proposed by the authors of [5, 6] in order to preserve a small amount of haze in distant objects. The reason is that if haze is completely removed the image may look unnatural and the perception of depth may be lost. The final equation for the computation of the transmission is

$$t(\boldsymbol{x}) = 1 - \omega \min_{c\in\{R,G,B\}} \min_{\boldsymbol{y}\in\Omega(\boldsymbol{x})} \frac{I^c(\boldsymbol{y})}{A^c}, \tag{14}$$

where ω is a constant ($0 < \omega \leq 1$) which is fixed to 0.95 in [5, 6].

Note that for small values of the factor

$$\min_{c\in\{R,G,B\}} \min_{\boldsymbol{y}\in\Omega(\boldsymbol{x})} \frac{I^c(\boldsymbol{y})}{A^c}$$

the new value of the transmission is very similar to the old one. But when this factor tends to 1 (the image values are close to the ambient light, which happens in distant points) the transmission is slightly higher than the one computed with Equation (12).

3.3 Refinement of the Transmission

The use of patches for the computation of the transmission map in Equation (14) produces some block effects in the result (see Figure 1). In order to refine this map He et al. propose to use a soft mapping algorithm [9]. However, in a later work [7] the same authors propose a more efficient refinement method based on the guided filter.

The guided filter takes as input the rough transmission map and the original haze image and produces a refined map whose edges follow the geometry of the image. The results are similar to the ones obtained with the soft mapping algorithm but the computation is much faster, since the computational complexity of the guided filter is linear with the size of the image when implemented using integral images [1].

Given a one-channel input (guidance) image I (in the case of color images, I is the intensity channel), and an initial transmission map t, the guided filter produces a refined map t'.

The key assumption of the guided filter is that the output t' is a linear transform of the guidance I in a patch Ω_k (a square window of size $r \times r$ pixels) centered at the pixel k

$$t'_i = a_k I_i + b_k, \forall i \in \Omega_k. \tag{15}$$

where i is a pixel index.

The coefficients a_k and b_k are determined by minimizing the difference between the filtered map and the original map. In particular, the following cost function is minimized for every patch

$$E(a_k, b_k) = \sum_{i\in\Omega_k} ((a_k I_i + b_k - t_i)^2 + \epsilon a_k^2), \tag{16}$$

where ϵ is a regularization parameter.

The solution of the minimization problem can be found using linear regression.

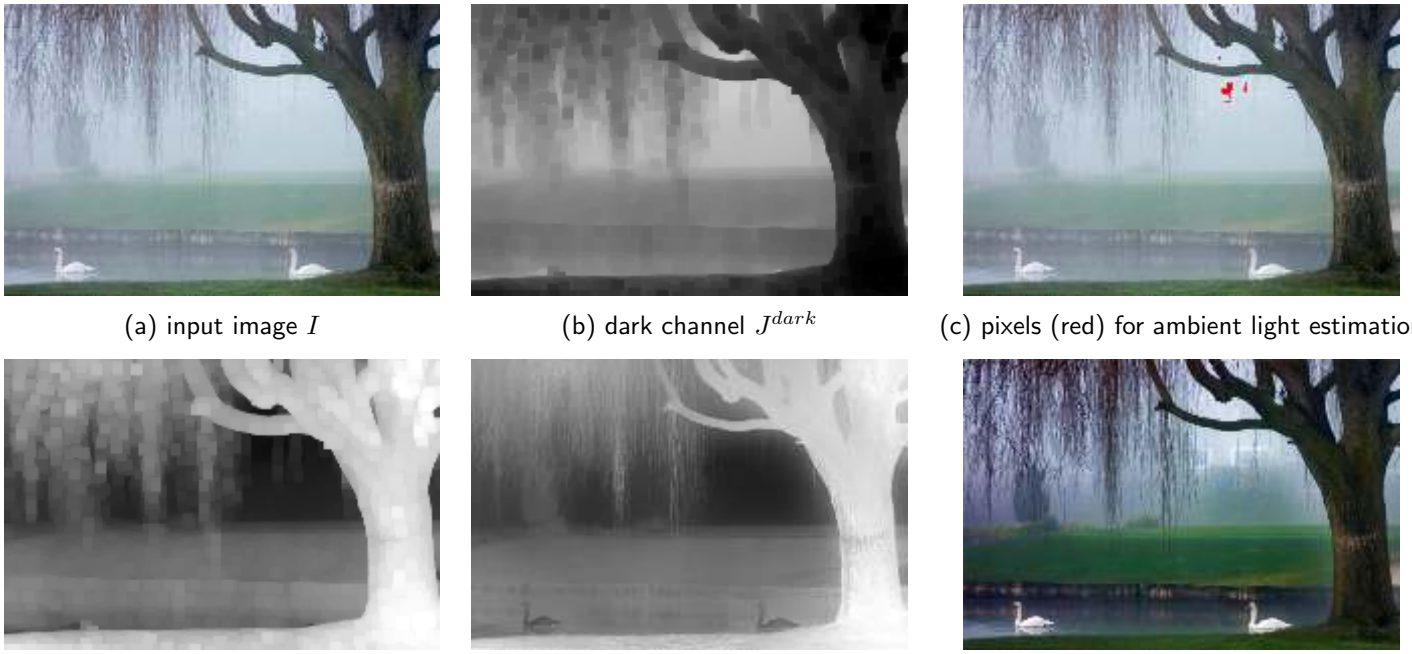

(a) input image I (b) dark channel J^{dark} (c) pixels (red) for ambient light estimation

(d) raw transmission map t (e) refined transmission map t' (f) dehazed image I'

Figure 1: Illustration of the successive steps of the method. First, the dark channel (b) is estimated. Then, the ambient light is estimated from the brightest pixels in the dark channel (illustration (c), pixels in red). The transmission is shown in (d), and the refined transmission in (e). Finally, (f) shows the dehazed image.

$$a_k = \frac{\frac{1}{r^2}\sum_{i\in\Omega_k} I_i t_i - \mu_k \bar{t}_k}{\sigma_k^2 + \epsilon}, \tag{17}$$

$$b_k = \bar{t}_k - a_k \mu_k, \tag{18}$$

where μ_k and σ_k^2 are the mean and variance of I in Ω_k and $\bar{t}_k = \dfrac{1}{r^2}\displaystyle\sum_{i\in\Omega_k} t_i$ is the mean of t in Ω_k.

Using Equations (17) and (18) the a_k and b_k values for each patch will be obtained. Since a pixel belongs to several patches, several values of t'_i are obtained through Equation (15). The average of all these values is used as the final output for t'_i.

$$t'_i = \frac{1}{r^2}\sum_{k\,:\,i\in\Omega_k} (a_k I_i + b_k) = \bar{a}_i I_i + \bar{b}_i, \tag{19}$$

where $\bar{a}_i = \dfrac{1}{r^2}\displaystyle\sum_{k\in\Omega_i} a_k$ and $\bar{b}_i = \dfrac{1}{r^2}\displaystyle\sum_{k\in\Omega_i} b_k$.

In [7] it is shown that the value of the regularization parameter ϵ determines the degree of smoothing of the filter. As ϵ increases only strong edges are preserved and the rest of the image is blurred.

The guided filter is implemented in Algorithms 2, 3 and 4.

3.4 Recovering the Scene Radiance

As commented in Section 2, once the ambient light $\boldsymbol{A}$ and the transmission map $t(\boldsymbol{x})$ have been estimated the scene radiance can be recovered through Equation (5). However, in practice, when the dividing factor $t(\boldsymbol{x})$ is close to zero the results for nearby pixels can by quite different and the obtained $\boldsymbol{J}$ is prone to noise. To prevent that, the values of $t(\boldsymbol{x})$ are clipped to a lower bound t_0 (by

Algorithm 2: Compute Integral Image (adapted from [3], Algorithm 1). The integral image (II) contains the accumulated values of the input image (I): $II(x,y) = \sum_{x' \le x, y' \le y} I(x',y')$.

Input : input image (one channel) I, of size $w \times h$
Output : integral image II, of size $w \times h$

$II(0,0) \leftarrow I(0,0)$
for $x \leftarrow 1$ **to** $w-1$ **do**
  $II(x,0) \leftarrow II(x-1,0) + I(x,0)$
for $y \leftarrow 1$ **to** $h-1$ **do**
  $s \leftarrow I(0,y)$ `//scalar accumulator`
  $II(0,y) \leftarrow II(0,y-1) + s$
  for $x \leftarrow 1$ **to** $w-1$ **do**
    $s \leftarrow s + I(x,y)$
    $II(x,y) \leftarrow II(x,y-1) + s$

Algorithm 3: Patch Averages

Input : input image (one channel) I
Output : image of average values I_{avg}. The output at each pixel is the average of input values in a patch centered at the pixel.
Parameters: r_r: radius of the patch ($r = 2r_r + 1$, patch size $r \times r$)

`// Auxiliary image for boundary handling: use convention dcb|abcdefgh|gfe`
$I' \longleftarrow BoundaryHandling(I, r_r)$ `//Size of` I': $(w+2r_r) \times (h+2r_r)$
$II' \longleftarrow IntegralImage(I')$ `//Algorithm 2`
for $y \leftarrow 0$ **to** $h-1$ **do**
  for $x \leftarrow 0$ **to** $w-1$ **do**
    $x' \leftarrow x + r_r$, $y' \leftarrow y + r_r$ `//coordinates of pixel` (x,y) `in integral image`
    `// The sum of all the values inside the patch can be computed with four operations using integral images (see [3] for details)`
    $I_{\text{avg}}(x,y) \leftarrow II'(x'+r_r, y'+r_r)$
    if $x' - r_r - 1 \ge 0$ **then**
      $I_{\text{avg}}(x,y) \leftarrow I_{\text{avg}}(x,y) - II'(x'-r_r-1, y'+r_r)$
    if $y' - r_r - 1 \ge 0$ **then**
      $I_{\text{avg}}(x,y) \leftarrow I_{\text{avg}}(x,y) - II'(x'+r_r, y'-r_r-1)$
    if $x' - r_r - 1 \ge 0$ ***and*** $y' - r_r - 1 \ge 0$ **then**
      $I_{\text{avg}}(x,y) \leftarrow I_{\text{avg}}(x,y) + II'(x'-r_r-1, y'-r_r-1)$
    $I_{\text{avg}}(x,y) \leftarrow I_{\text{avg}}(x,y)/(2r_r+1)^2$

default 0.1), which implies that a certain amount of haze is preserved in regions with dense haze. The final equation for recovering the radiance is

$$\boldsymbol{J}(\boldsymbol{x}) = \frac{\boldsymbol{I}(\boldsymbol{x}) - \boldsymbol{A}}{\max(t(\boldsymbol{x}), t_0)} + \boldsymbol{A}. \tag{20}$$

Algorithm 4: Guided Filter

Input : rough transmission map t
Input : input image (intensity channel) I (size $w \times h$)
Output : refined transmission map t'
Parameters: r_r: radius of the patch ($r = 2r_r + 1$, patch size $r \times r$), ϵ: regularization parameter

// The symbols $\odot$ and $\oslash$ denote pixel-wise product and division, respectively
$I \leftarrow I/255$ //normalize values to [0, 1]
// Image of averages of I values in $r \times r$ patches
$\mu_I \longleftarrow PatchAverages(I, r)$ //Algorithm 3
// Image of averages of I^2 values in $r \times r$ patches
$\mu_{I^2} \longleftarrow PatchAverages(I \odot I, r)$ //Algorithm 3
// Image of variances of I values in $r \times r$ patches
$\text{var}_I \leftarrow \mu_{I^2} - \mu_I \odot \mu_I$
// Image of averages of t values in $r \times r$ patches
$\mu_t \longleftarrow PatchAverages(t, r)$ //Algorithm 3
// Image of averages of $I \cdot t$ values in $r \times r$ patches
$\mu_{It} \longleftarrow PatchAverages(I \odot t, r)$ //Algorithm 3
// Image of covariances of I and t values in $r \times r$ patches
$\text{covar}_{It} \leftarrow \mu_{It} - \mu_I \odot \mu_t$
// Image of a coefficients
$a \leftarrow \text{covar}_{It} \oslash (\text{var}_I + \epsilon \cdot \text{Identity})$ //Equation (17)
// Image of b coefficients
$b \leftarrow \mu_t - a \odot \mu_I$ //Equation (18)
// Image of averages of a values in $r \times r$ patches
$\mu_a \longleftarrow PatchAverages(a, r)$ //Algorithm 3
// Image of averages of b values in $r \times r$ patches
$\mu_b \longleftarrow PatchAverages(a, r)$ //Algorithm 3
// Refined map
$t' \leftarrow \mu_a \odot I + \mu_b$ //Equation (19)

3.5 Parameters of the Method

In this section we summarize the parameters of the dehazing method, and the default values proposed by the authors.

- s: size of the square patches used to compute the dark channel in Equation (6). In practice, we use as parameter the *radius* of the patch s_r ($s = 2s_r + 1$). Default: $s_r = 7$ (patch size of 15×15 pixels).
- p: percentage of pixels used to estimate the ambient light in Algorithm 1. Default: $p = 0.1\%$.
- ω: correction factor for transmission map estimation in Equation (14). Default: $\omega = 0.95$.
- r: size of the square patches used in the guided filter. In practice, we use as parameter the *radius* of the patch r_r ($r = 2r_r + 1$). Default: $r_r = 30$ (patch size of 61×61 pixels).
- ϵ: regularization parameter of the guided filter. Default: $\epsilon = 0.0001$.

- t_0: minimum allowed value of the transmission map in Equation (20). Default: $t_0 = 0.1$.

In Section 4 several experiments have been performed analyzing the effect of the different parameters on the dehazing results.

3.6 Dehazing Algorithm

Algorithm 5 describes the complete dehazing algorithm based on the dark channel prior.

Algorithm 5: Dark Channel Prior (DCP) Dehazing

Input : input image $\boldsymbol{I}$
Output : dehazed image $\boldsymbol{I'}$
Parameters: (described in Section 3.5): s_r, p, ω, r_r, ϵ, t_0

`//Estimate the dark channel (approximate` J^c `by` I^c `in Equation (6))`
1 $J^{\text{dark}}(\boldsymbol{x}) = \min_{\boldsymbol{y}\in\Omega(\boldsymbol{x})} \min_{c\in\{R,G,B\}} I^c(\boldsymbol{y})$
`//Estimate ambient light (Algorithm 1)`
2 $\boldsymbol{A} = \text{EstimateAmbientLight}(\boldsymbol{I}, J^{\text{dark}}, p)$
`//Compute Transmission Map (Equation (14))`
3 $t(\boldsymbol{x}) = 1 - \omega \min_{c\in\{R,G,B\}} \min_{\boldsymbol{y}\in\Omega(\boldsymbol{x})} \frac{I^c(\boldsymbol{y})}{A^c}$
`//Refine Transmission Map (Algorithm 4)`
4 $I = \text{IntensityChannel}(\boldsymbol{I})$ `//Average of RGB channels`
5 $t' = \text{GuidedFilter}(t, I, r_r, \epsilon)$
`//Recover Scene Radiance (Equation (20))`
6 $\boldsymbol{I'}(\boldsymbol{x}) = \frac{\boldsymbol{I}(\boldsymbol{x}) - \boldsymbol{A}}{\max(t(\boldsymbol{x}), t_0)} + \boldsymbol{A}$

3.7 Computational Complexity

The computational complexity of Algorithms 1 to 4 is $O(N)$, where N is the number of pixels in the image. On the other hand, the computation of the dark channel and the transmission map (lines 1 and 3 in Algorithm 5) takes $O(N(2r+1)^2)$ operations, where r is the radius of the square patches used in Equations (6) and (14). Since all the operations involving a single pixel are independent from the rest, they can be easily parallelized. In our C++ implementation, this is achieved through the use of OpenMP directives.

4 Experiments

In our experiments, we found that the default parameters work well for most images. In the following, we concentrate on images where we observed that the result is less robust to a change in the parameters.

We first present experiments on the estimation of the dark channel and the ambient light. Those two steps have a strong impact on the result. Then, we analyze the steps computing and refining the transmission map, and recovering the scene radiance.

4.1 Dark Channel and Ambient Light Estimation

We show in Figure 2 the effect of the patch size parameter. Larger patches will often underestimate the depth, by propagating, in the dark channel image, the low image value to the closest objects.

For example the haze nearby the tree in Figure 2 is not as well removed as in the regions further away from the tree. This effect is partially corrected by the refinement step, but not completely: compare the filtered transmission maps in (c), (f) and (i). For this reason, the output image has a halo around dark objects. This halo effect is further discussed in Section 4.2.

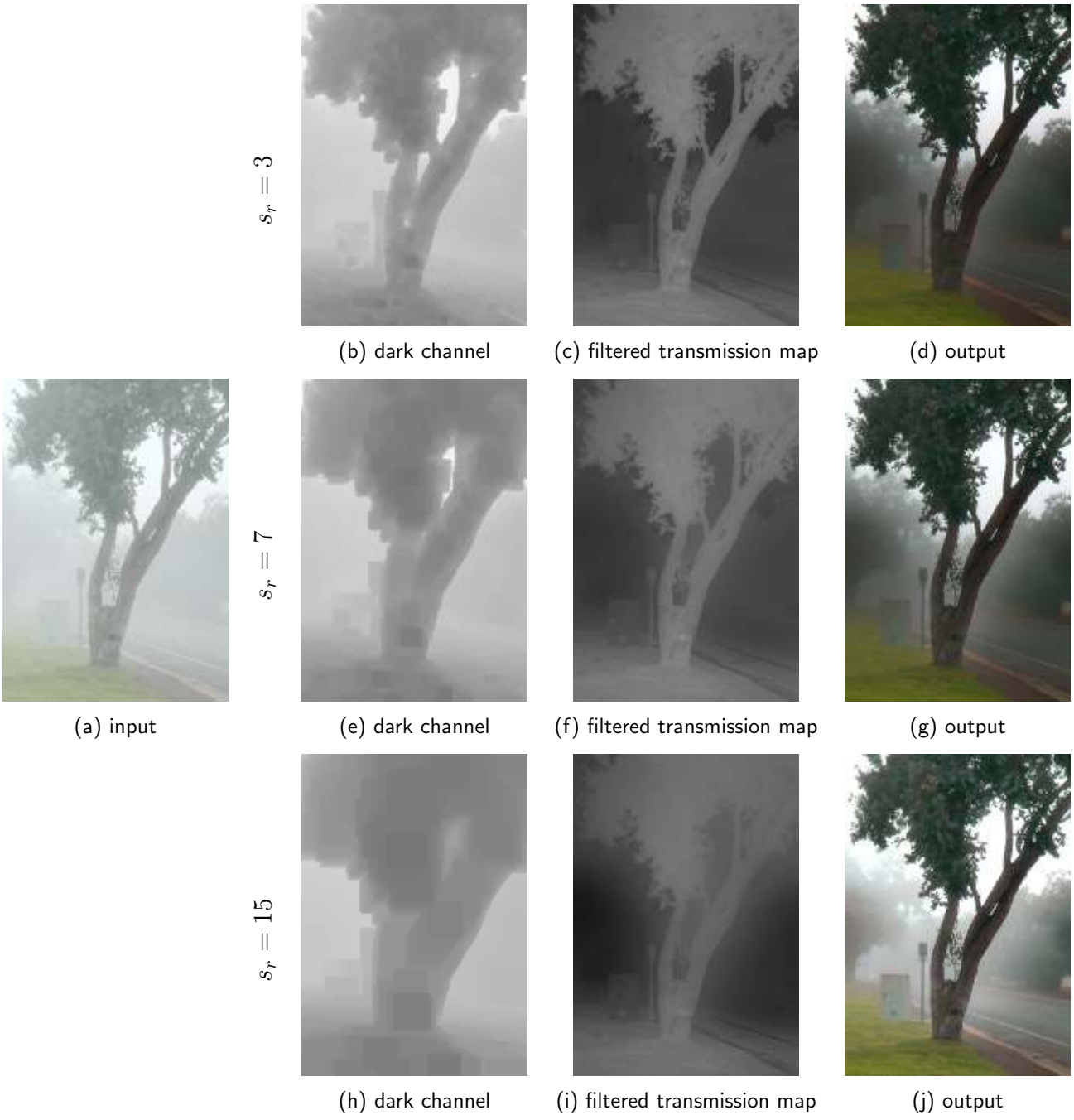

Figure 2: Effect of the parameter s_r on the dark channel estimation. Three values are shown here: $s_r = 3$ on the top row, $s_r = 7$ in the center row (the default value for this parameter), and $s_r = 15$ on the bottom row. The patch is a square of width $2s_r + 1$ pixels.

On the other hand, Figure 3 shows that a larger patch size prevents the over-correction of whitish objects. Indeed, for these objects the value in the dark channel is high and therefore its transmission is low, hinting at a large distance from the camera which is not necessarily true (see e.g. the stones at the bottom of the image). The use of larger patch sizes increases the value of the transmission for these objects, reducing the amount of the correction in Equation (20). Nevertheless, the haze

removal for the furthest regions of the scene is also reduced, as seen in the buildings in the top part of the image.

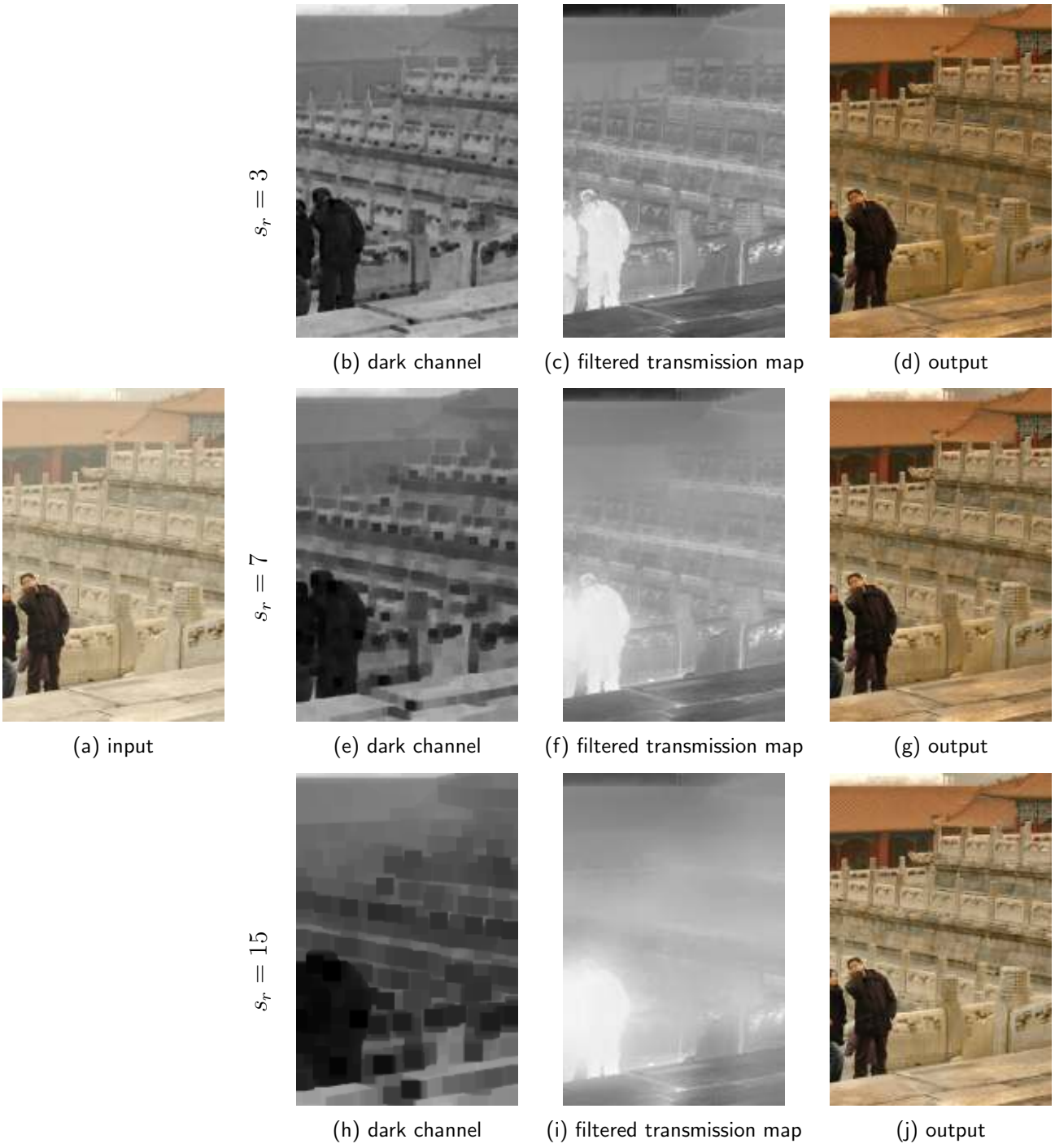

Figure 3: Effect of the parameter s_r on the dark channel estimation. Similarly to Figure 2, three values are shown here: $s_r = 3$ on the top row, $s_r = 7$ in the center row (the default value for this parameter), and $s_r = 15$ on the bottom row.

Figure 4 shows another example where the dark channel prior does not hold. In this image, one windowless gray side of a building is illuminated by the sunlight. This region in the dark channel is very bright, which results in a very low transmission value, even lower than the sky. The output image is displayed in Figure 5(b). Another consequence of the incorrect estimation of the transmission concerns the ambient light estimation, as illustrated in Figure 5. Since the method estimates the ambient light from the pixels with the lowest transmission, it uses the building region (pixels marked

in red in Figure 5(a)). The ambient light is then wrongly estimated with a yellow tint, and this, in consequence, gives a blue tint to the corrected image, as seen in Figure 5(b). To evaluate the effect of a more correct estimation of the ambient light on the result, we used the mean of a manually selected region from the input image. This region is depicted with a green rectangle in Figure 5(a). The result of using this estimated ambient light for the dehazing is shown in Figure 5(c). With a more accurate ambient light estimation, the blue color cast is removed. However, we observe that in this case there is an excessive enhancement of the image, which produces color saturation in the building on the left and makes the noise visible in the sky. This is because A is not computed from the highest values in the image, which leads to saturation (the dehazing operation is essentially a contrast amplification after a color correction, see Equation (20)).

(a) input (b) dark channel (c) filtered transmission

Figure 4: Example image where the dark channel prior does not hold. The default values are used for the parameters.

(a) Input image (b) Dehazing result (default) (c) Dehazing result (with different A)

Figure 5: Effect of the ambient light estimation A on the result. In this image, the pixels used by default for the ambient light estimation are located on a bright building close to the camera. These pixels are marked in red in image (a). The corresponding dehazed image is shown in (b). Note the blue color cast of the image. On the other hand, using the pixels inside the green rectangle, displayed in (a), the ambient light is correctly estimated, leading to a result that doesn't exhibit the blue cast (c).

4.2 Computation and Refinement of the Transmission map

In Figure 6, we illustrate the effect of the guided filter parameters r_r and ϵ on the filtering of the transmission map. A larger radius makes the halo less visible, but also decreases the strength of the correction (looking at the output results (e), the images on the right have more remaining haze than the ones on the left). Regarding ϵ, we observe that when it is increased the transmission map becomes more blurry, its highest values are decreased while its lowest values are increased. As a consequence, the contrast between the brightest and the darkest objects of the image is increased, which produces a stronger dehazing effect.

In order to further study the halo artifact introduced by the method (as already pointed out in Section 4.1), in Figure 7 we display profiles of the results obtained by dehazing the input image of Figure 6 using different values of the parameters. We observe that although the input image is almost flat in the displayed part, most corrected versions exhibit a strong gradient. This gradient

can be reduced using a larger patch size r to filter the transmission map (see the brown profile in the figure, corresponding to $r_r = 60$) but, as remarked before, the dehazing effect is also reduced. Additional examples of the halos produced by the method are shown in Figure 8. It can be seen for example around the branches in images (d) and (e), and around the tower in (f). These images are computed using the default parameters of the method.

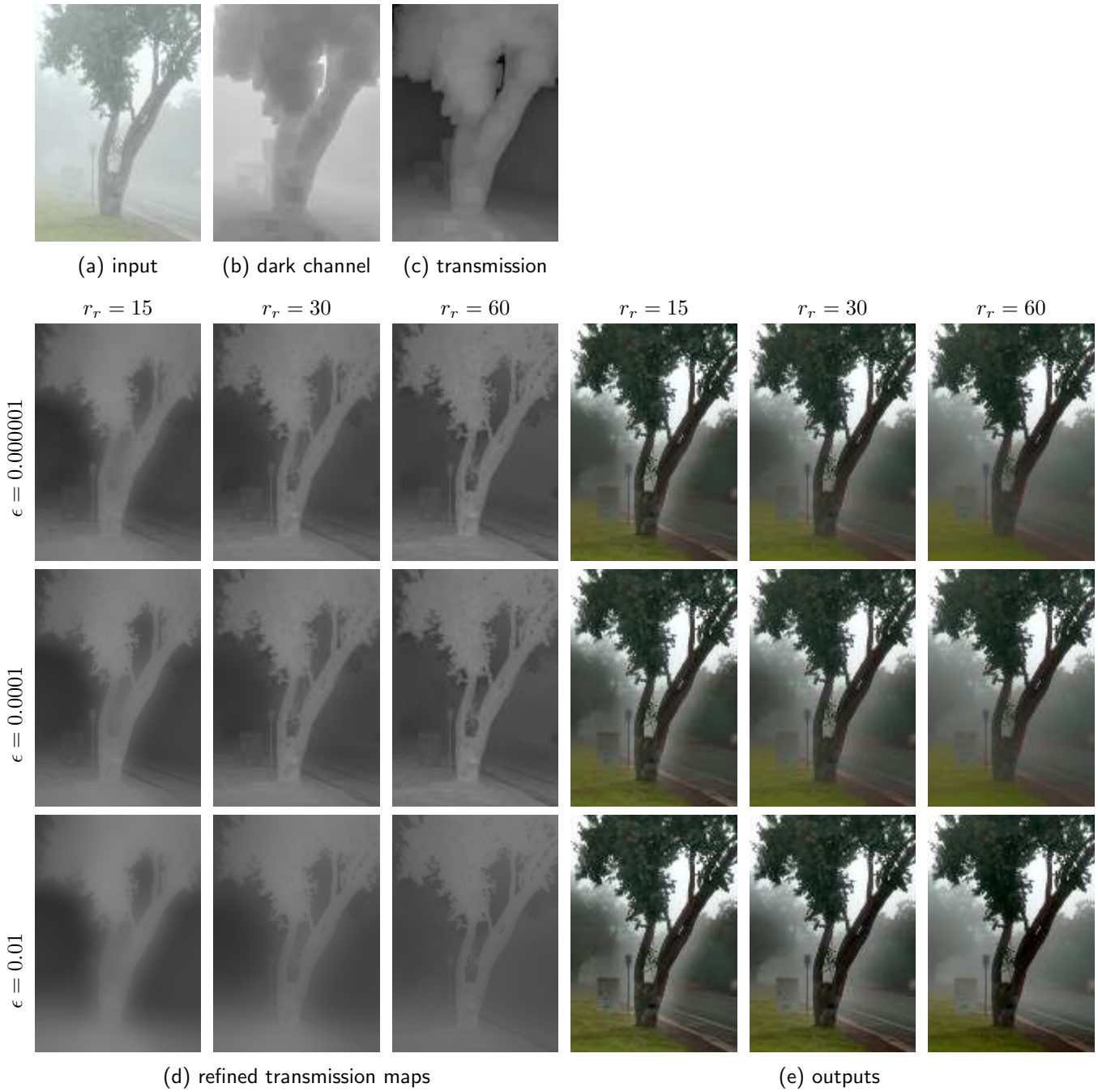

Figure 6: Effect of the radius parameter r_r of the guided filter. With larger radii, the halo become less visible, but the dehazing strength decreases too. On the other hand, with bigger ϵ values the edges of the input image are better preserved in the transmission map, while it becomes more blurry as ϵ decreases. As a consequence the dehazing effect is stronger with bigger values of the parameter.

In Figure 9, we show the effect of varying the parameters t_0 and ω. In this image, the contrast enhanced sky in the output exhibits color banding and JPEG compression artifacts. The smaller t_0, the stronger the effect. On the other hand, as ω decreases the effect is less visible.

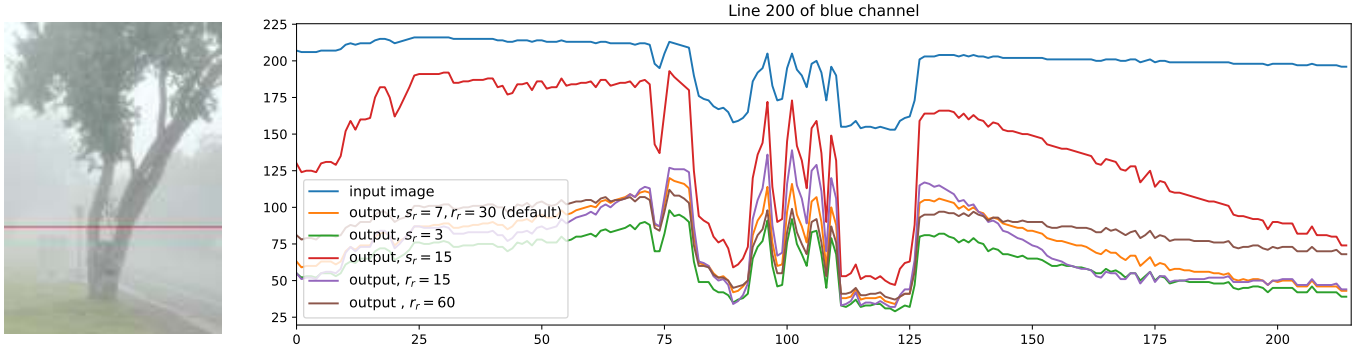

Figure 7: Profiles (line 200, shown in red on the left) for several images: the input and output for different parameters. On the right side of the plot (from pixel 125), the halo is clearly visible: although the input image is almost flat in this region of roughly constant depth (blue line), most corrected versions exhibit a strong gradient, especially near the tree's trunk (pixels 110-125).

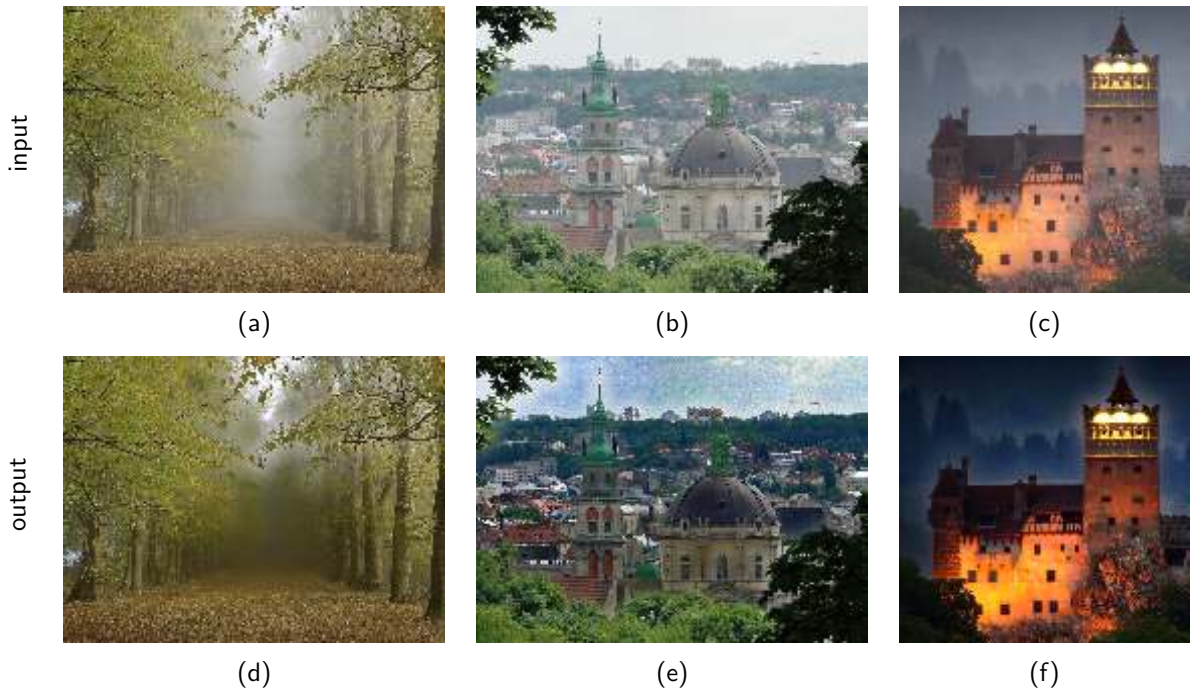

Figure 8: Example result with visible halos, using the default parameters.

Concluding remarks.

- First, the hypothesis that haze-free objects have pixels with low values (the dark channel prior) is not always verified. This is the case in particular for bright objects. The method therefore tends to over correct them (they are considered hazy). Increasing the radius s_r of the patch used to compute the dark channel will help in this regard. However this will also prevent a good correction of the haze enclosed between low-depth objects, e.g. between tree branches.

  Another consequence of the failure of the dark channel prior is the incorrect estimation of the ambient light, which may introduce a color cast in the results.

- Second, the method often produces a halo near objects with contrasted atmospheric depths: the dehazing is generally weaker around objects from the foreground. Different combinations of the parameters s_r and r_r may help to reduce this effect, at the expense of a less dehazed result.

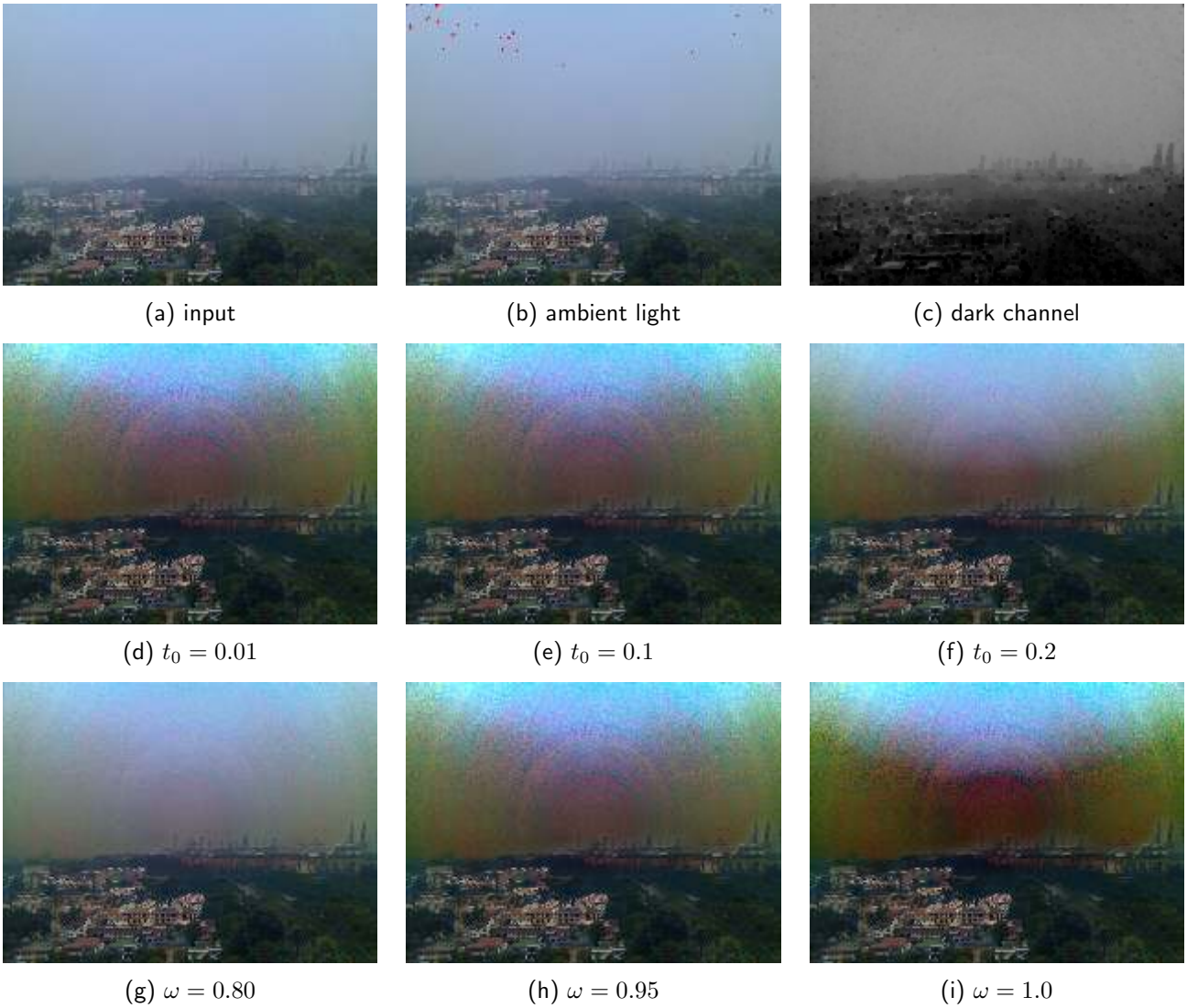

(a) input (b) ambient light (c) dark channel

(d) $t_0 = 0.01$ (e) $t_0 = 0.1$ (f) $t_0 = 0.2$

(g) $\omega = 0.80$ (h) $\omega = 0.95$ (i) $\omega = 1.0$

Figure 9: Effect of the parameters t_0 and ω on the output. The rest of the parameters take their default values.

- Finally, the correction can be too strong, which makes noise, banding and JPEG compression artifacts more visible. This effect is often observed in the sky. The distortions can be reduced with an appropriate value of the parameters ω and t_0.

5 Adaptation to Underwater Images (UDCP)

A slight variation of Algorithm 5 was proposed in 2013 by Drews et al. [2] for the estimation of transmission maps in underwater images. They observed that the information provided by the red channel of these images was not reliable due to the strong attenuation of its values, and proposed to ignore it in the computation of the dark channel. Therefore, line 1 of Algorithm 5 is replaced by

$$J^{\text{dark}}(\boldsymbol{x}) = \min_{\boldsymbol{y}\in\Omega(\boldsymbol{x})} \min_{c\in\{G,B\}} I^c(\boldsymbol{y}).$$

Drews et al. assert that this simple modification permits to obtain much accurate transmission maps in underwater scenes, and therefore a better estimation of the depth of the objects in the scene. This is confirmed by our experiments (see Figure 10). Although in some cases the transmission maps obtained by the original DCP method and by Underwater DCP (UDCP) are similar (see the two

first rows in the figure), in most cases UDCP outperforms DCP. It must be noted that, as happens with DCP, the presence of bright objects disrupts the estimation, since the prior is no longer valid. This happens for example with the sand in the third row image: UDCP estimates low transmission values, suggesting that this part of the image is far from the camera, but it is indeed close to it. A similar error is observed in the arm of the scuba diver at the bottom of the figure.

Figure 11 compares the results of applying the dehazing equation (20) to the transmission map and ambient light estimated using UDCP and DCP. We observe that the UDCP results tend to be darker, may contain color artifacts and some parts of the images are excessively enhanced. The reason is the incorrect ambient light estimation and the fact that the transmission can take very low values in some parts of the scene, leading to a very strong enhancement.

Figure 12 shows that these problems can be mitigated with a better estimation of the ambient light and the fine tuning of the parameters that limit the values of the transmission map. A simple modification of Algorithm 1 permits to improve the estimation: saturated pixels are excluded from the estimation. We consider that a pixel is saturated if any of its channels reaches the value 255. The pixels marked in red in Figure 12(a) are the ones used for the estimation in the original algorithm, while the pixels marked in blue are used when applying this modification. The corresponding dehazed images are shown in (b) and (c). The result can be improved (see image (d)) by limiting the strength of the enhancement, setting parameter ω to a lower value, as suggested in Section 4.2.

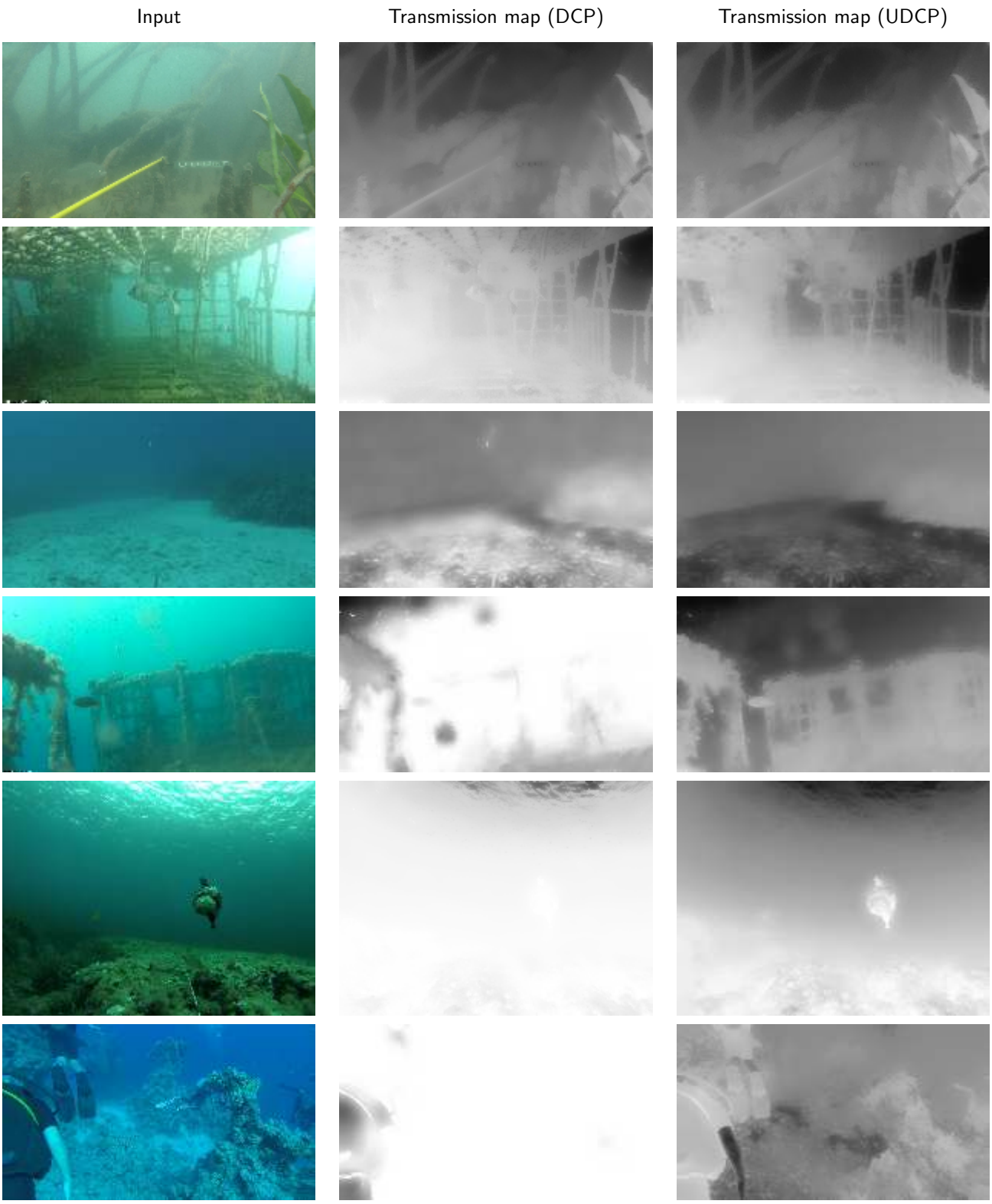

Figure 10: Underwater images and transmission maps estimated using the DCP and the UDCP priors.

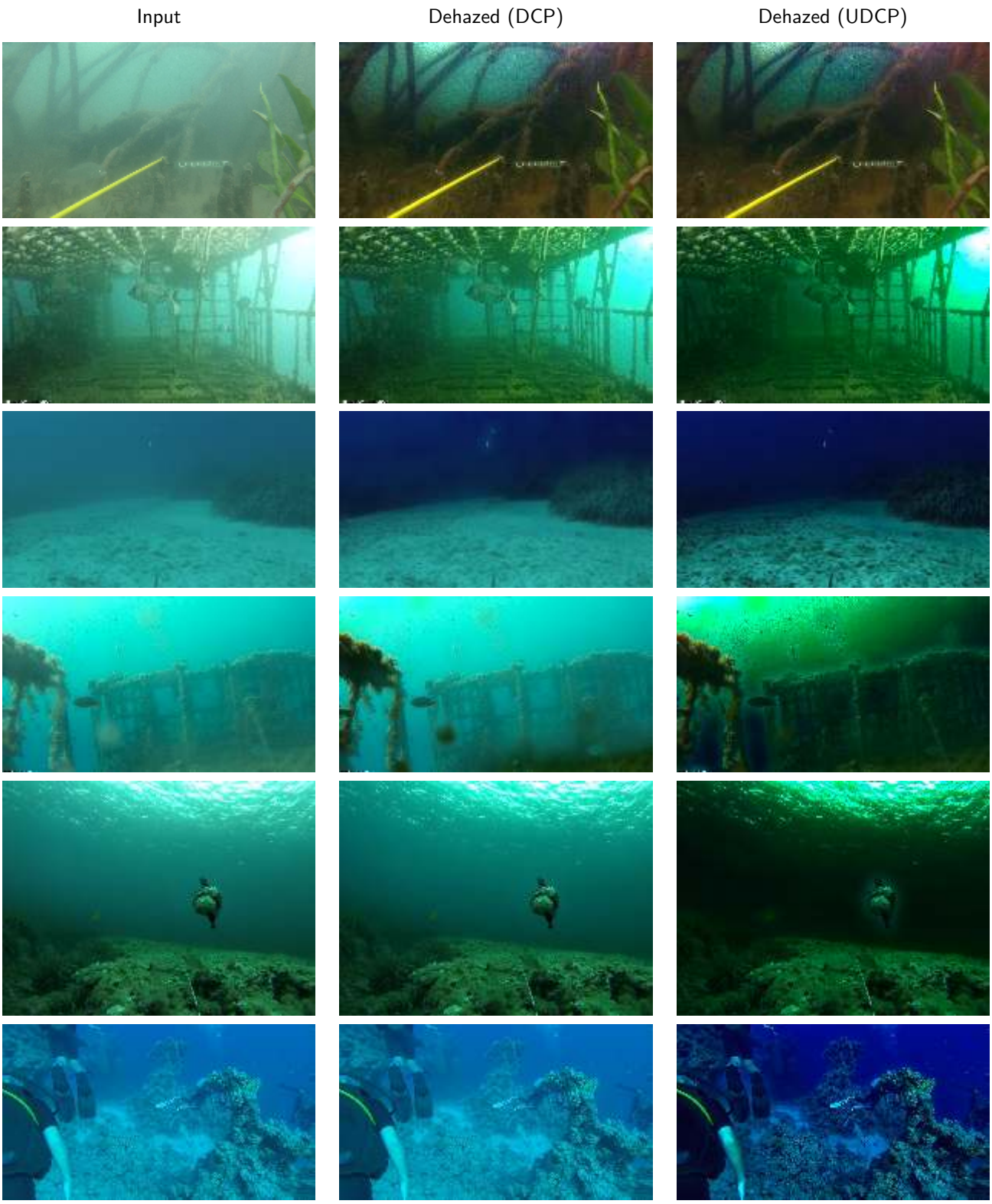

Figure 11: Underwater images and dehazing results using the DCP and the UDCP priors.

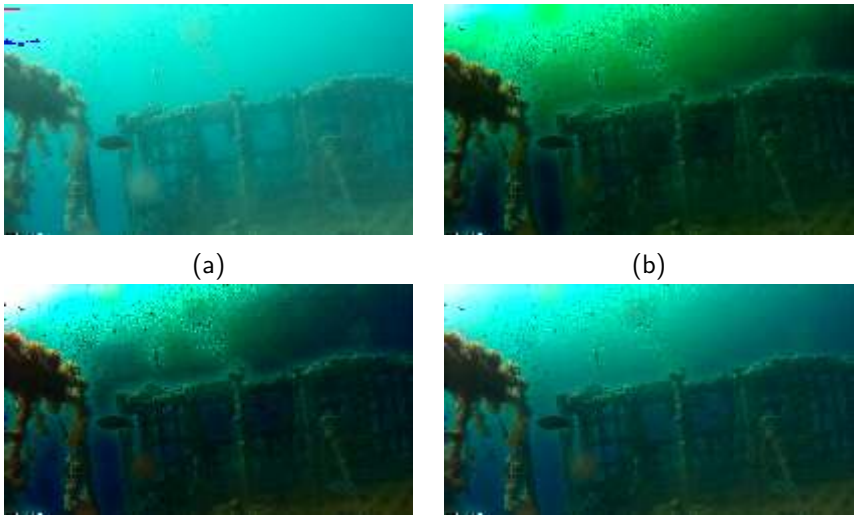

Figure 12: Improving the dehazing result of UDCP: (a) Original image with the default pixels used for ambient light estimation marked in red. In blue, the pixels used for the estimation when saturated pixels are excluded. (b) Dehazing result using the default parameters of UDCP and the default ambient light estimation (using red pixels in (a)). (c) Dehazing result using the default parameters of UDCP and ambient light estimation excluding saturated pixels (using blue pixels in (a)). (d) Dehazing result using ambient light estimation excluding saturated pixels (using blue pixels in (a)), and $\omega = 0.8$ (the rest of parameters take their default values).

6 Conclusions

In this paper we have given a full account of the Dark Channel Prior method for image dehazing, described its parameters and analyzed how their variation influences the final result.

Although this is one of the most popular and cited methods for dehazing, and in general it gives good results, we have shown its limitations in the experimental section. In particular, we have observed the appearance of halos, color cast and excessive enhancement for some images.

Finally, we have displayed a variation of the method when applied to underwater images. Although in this case the obtained depth estimations are good in general, the dehazed results often exhibit color artifacts and excessive enhancement of the noise, which can be mitigated with a better estimation of the ambient light and by tuning the default parameters of the method.

Acknowledgements

The first author has been partially sponsored by project PID2021-125711OB-I00, financed by MCIN / AEI / 10.13039 /501100011033 / FEDER, EU. His work has also been partially sponsored and promoted by the Comunitat Autonoma de les Illes Balears through the through the Servei de Recerca i Desenvolupament and the Conselleria d'Educació i Universitats and the Conselleria de Economia, Hisenda i Innovació and by the European Union- Next Generation UE via Plans complementaris del Pla de Recuperació, Transformació i Resiliència (PRTR-C17-I1) and by the European Union-Next Generation UE (BIO/002A.1). Nevertheless, the views and opinions expressed are solely those of the author or authors, and do not necessarily reflect those of the European Union or the European Commission. Neither the European Union nor the European Commission are to be held responsible.

Image Credits

 from [13].

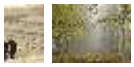 from [5].

 from [14].

 from [12].

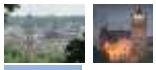 unknown author.

 Geroithe Chia (Flickr) CC BY-SA 2.0.

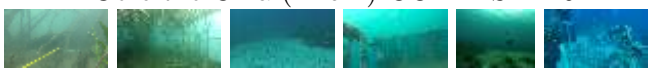 from IMEDEA[2].

References

[1] F. C. Crow, *Summed-Area Tables for Texture Mapping*, in Conference on Computer Graphics and Interactive Techniques, 1984, pp. 207–212, https://doi.org/10.1145/800031.808600.

[2] P. Drews, E. Nascimento, F. Moraes, S. Botelho, and M. Campos, *Transmission Estimation in Underwater Single Images*, in IEEE International Conference on Computer Vision Workshops, 2013, pp. 825–830, https://doi.org/10.1109/ICCVW.2013.113.

[3] G. Facciolo, N. Limare, and E. Meinhardt-Llopis, *Integral Images for Block Matching*, Image Processing On Line, 4 (2014), pp. 344–369, https://doi.org/10.5201/ipol.2014.57.

[4] R. Fattal, *Single Image Dehazing*, ACM Transactions on Graphics (TOG), 27 (2008), pp. 1–9, https://doi.org/10.1145/1360612.1360671.

[5] K. He, J. Sun, and X. Tang, *Single Image Haze Removal Using Dark Channel Prior*, in IEEE Conference on Computer Vision and Pattern Recognition (CVPR), vol. 33, 2009, pp. 1956–1963, https://doi.org/10.1109/CVPR.2009.5206515.

[6] K. He, J. Sun, and X. Tang, *Single Image Haze Removal Using Dark Channel Prior*, IEEE Transactions on Pattern Analysis and Machine Intelligence, 33 (2010), pp. 2341–2353, https://doi.org/10.1109/TPAMI.2010.168.

[7] ——, *Guided Image Filtering*, IEEE Transactions on Pattern Analysis and Machine Intelligence, 35 (2012), pp. 1397–1409, https://doi.org/10.1007/978-3-642-15549-9_1.

[8] J. S. Jaffe, *Computer Modeling and the Design of Optimal Underwater Imaging Systems*, IEEE Journal of Oceanic Engineering, 15 (1990), pp. 101–111, https://doi.org/10.1109/48.50695.

[9] A. Levin, D. Lischinski, and Y. Weiss, *A Closed-Form Solution to Natural Image Matting*, IEEE Transactions on Pattern Analysis and Machine Intelligence, 30 (2007), pp. 228–242, https://doi.org/10.1109/CVPR.2006.18.

[10] B. McGlamery, *A Computer Model for Underwater Camera Systems*, in Ocean Optics VI, vol. 208, SPIE, 1980, pp. 221–231.

[2]Mediterranean Institute of Advanced Studies (CSIC-UIB), Spain, https://imedea.uib-csic.es/en/

[11] S. G. Narasimhan and S. K. Nayar, *Vision and the Atmosphere*, International Journal of Computer Vision, 48 (2002), pp. 233–254, https://doi.org/10.1023/A:1016328200723.

[12] Y. Y. Schechner, S. G. Narasimhan, and S. K. Nayar, *Instant Dehazing of Images Using Polarization*, in IEEE Computer Society Conference on Computer Vision and Pattern Recognition (CVPR), vol. 1, 2001, pp. I–I, https://doi.org/10.1109/CVPR.2001.990493.

[13] R. T. Tan, *Visibility in Bad Weather from a Single Image*, in IEEE Conference on Computer Vision and Pattern Recognition (CVPR), 2008, pp. 1–8, https://doi.org/10.1109/CVPR.2008.4587643.

[14] X. Zhao, *Single Image Dehazing Using Bounded Channel Difference Prior*, in IEEE/CVF Conference on Computer Vision and Pattern Recognition (CVPR), 2021, pp. 727–735, https://doi.org/10.1109/CVPRW53098.2021.00082.